

1 **Enhancing the binding affinity of an underperforming WW domain using** 2 **structural and dynamic-based design.**

3
4 Jin Lu^{1#}, Mohammad Imtiazur Rahman^{2#}, I. Can Kazan^{1#}, Nicholas R. Halloran², Andrey A.
5 Bobkov³, S. Banu Ozkan^{1*} and Giovanna Ghirlanda^{2*}
6

7 ¹Department of Physics and Center for Biological Physics, Arizona State University, Tempe, Arizona 85287, United States

8 ²School of Molecular Sciences, Arizona State University, Tempe, Arizona 85287, United States

9 ³Conrad Prebys Center for Chemical Genomics, Sanford Burnham Prebys Medical Discovery Institute, La Jolla, California 92037,
10 United States

11 [#]These authors contributed equally to the paper

12 ^{*}Corresponding authors: Banu.Ozkan@asu.edu; gghirlanda@asu.edu
13
14
15

16 **Abstract**

17 Proteins gain optimal fitness such as foldability and function through evolutionary
18 selection. However, classical studies have found that evolutionarily designed protein sequences
19 alone cannot guarantee foldability, or at least not without considering local contacts associated
20 with the initial folding steps. We previously showed that foldability and function can be restored
21 by removing frustration in the folding energy landscape of a model WW domain protein, CC16,
22 which was designed based on Statistical Coupling Analysis (SCA). Substitutions ensuring the
23 formation of five local contacts identified as “on-path” were selected using the closest homolog
24 native folded sequence, N21. Surprisingly, the resulting sequence, CC16-N21, bound to group 1
25 peptides, while N21 did not. Here, we identified single-point mutations that enable N21 to bind a
26 group 1 peptide ligand through structure and dynamic-based computational design. Comparison
27 of the docked position of the CC16-N21/ligand complex with the N21 structure showed that
28 residues at positions 9 and 19 are important for peptide binding, whereas the dynamic profiles
29 identified position 10 as allosterically coupled to the binding site and exhibiting different dynamics
30 between N21 and CC16-N21. We found that swapping these positions in N21 with matched
31 residues from CC16-N21 recovers nature-like binding affinity to N21. This study validates the use
32 of dynamic profiles as guiding principles for affecting the binding affinity of small proteins.

33 **Key Words:** Energy landscape, WW domain, CC16, SCA, N21, CC16-N21, group 1 peptide,
34 Structure and dynamic-based design, Binding affinity
35

36 **Introduction**

37 Protein sequences encode the necessary information for folding and function and are
38 optimized through evolutionary pressure specific to the environment.¹⁻⁴ Within a protein family,
39 multiple sequence alignment (MSA) reveals which residues are crucial through conservation (i.e.,
40 amino acid position preference) and co-evolution statistics, which can be used to predict mutation
41 effects.⁵⁻¹¹

42 Classic folding and binding studies have focused on WW domains, one of the most
43 abundant independently folded protein domains in nature, because of their biological importance
44 in regulating transcription, apoptosis, and ubiquitylation by binding to proline-rich peptides.¹²⁻¹⁷
45 Due to its importance, the artificial WW domain sequences were designed using evolutionary
46 inferences methods by incorporating co-evolution and conservation. While successful in designing
47 artificial sequences of WW domains that are capable of folding like their natural counterparts, a
48 significant proportion (approximately two-thirds) of these designed sequences failed to fold
49 correctly^{3,7}. In our previous work, we showed that in those designed sequences non-foldability
50 was due to frustration: the N-terminal β -hairpin turn would not form correctly due to strong non-
51 native local contacts. Conversely, explicit consideration of the early folding steps restored
52 foldability by reducing frustration¹⁸. We identified five contacts that stabilize the nascent β -
53 hairpin, and grafted them from a foldable natural homologous sequence, N21, to an unfolded,
54 designed sequence, CC16. This newly designed variant, CC16-N21, folds and binds the group 1
55 proline-rich target ligand with binding affinity comparable with natural WW domains ($K_d = 71$
56 μM)^{7,18}. On the other hand, the native sequence N21, which shares 58% sequence similarity with
57 CC16-N21, shows no affinity to this peptide ligand, even though it is much more stable than CC16-
58 N21 to thermal denaturation ($T_m 46.8^\circ\text{C}$ vs 22.4°C)¹⁸.

59 In this current study, we extend our previous design and characterization of WW-based
60 variants to provide insights binding mechanism of WW domain. We aim to investigate the balance
61 between folding and binding as more stable native sequence N21 exhibits poor binding affinity
62 compared to less stable but better binder, designed CC16-N21. Our goal is to identify mutations
63 that can modulate the binding affinity of the native N21 sequence to group 1 peptides. Thus, we
64 perform a comprehensive structural and dynamic analysis comparing N21 and CC16-N21. We
65 utilized our docking method, Adaptive BP-Dock, to sample the binding trajectories with group 1
66 peptide (EYPPYPPPPYPSG), and compared the lowest energy bound poses^{9,19,20}. Our analysis
67 revealed critical interactions between two tyrosine residues (9Y and 19Y) in CC16-N21 that were

68 absent in the N21 sequence, highlighting their role in binding. To further explore the impact of
69 these differences, we introduced tyrosine residues at corresponding positions in the N21 sequence,
70 generating three mutants: H9Y, H19Y, and the double mutant H9YH19Y (Figure S1).

71 Additionally, we explored the conformational differences between N21 and CC16-N21 in
72 the unbound state using dynamic flexibility index (DFI) analysis. DFI is a position-specific metric
73 that computes each residue position's response fluctuation to external perturbations (i.e., random
74 Brownian kick) occurring on the protein chain., DFI is related to conformational entropy per
75 residue position²¹. Positions exhibiting low DFI values (i.e., a DFI percentile value lower than 0.2)
76 are classified as hinges. Hinges are stable locations within the 3-D interaction network of a protein,
77 and they do not deviate from their mean when external perturbations occur on the protein.
78 However, due to their extensive interaction network, they can transfer perturbations to the rest of
79 the protein. These rigid hinge's locations can act like joints in a skeleton, mediating the collective
80 motion of the protein, and have been shown to be important for function²¹⁻²⁵. Our previous protein
81 evolution studies showed that proteins modulate function through a hinge-shift mechanism in
82 which increases in flexibility of certain hinges (i.e., hinge losses) are compensated by rigidification
83 at other distal flexible sites (i.e., new hinge formation) through mutations during evolution²⁴⁻²⁶. In
84 the present study, we used this hinge-shift mechanism as a novel conformational dynamics-based
85 computational design approach to find distal sites (i.e., allosteric mutation sites) from the binding
86 residues to modulate binding affinity through altering dynamics. Thus, we rationally mold the
87 protein flexibility profile of the N21 based on changes in hinge location upon mutation, then
88 deliberately weigh and alter the dynamics (assessed by DFI profiles) of the designed N21
89 sequences towards the dynamics of better binder CC16-N21 following the similar dynamics
90 designed approach in our other studies^{11,24,25,27}. To this end, we compared the DFI profiles of N21
91 and CC16-N21: we found a drastic difference in the flexibility of two distal sites (P16, T10),
92 suggesting that they may allosterically modulate binding through alteration of dynamics. Position
93 16 is as proline in N21 and CC16-N21, while position 10 is T in N21 and H in CC16-N21. We
94 evaluated this hinge-shift location's contribution to binding by swapping these residues in variant
95 T10H and examining the resulting binding profile computationally. Finally, all variants designed
96 by either structural or dynamic approaches were expressed and characterized experimentally.
97 These two orthogonal design approaches show that not only the specific interactions of the residues

98 of the binding site, but distal sites can also modulate the binding of the WW domain through
99 dynamic allostery.

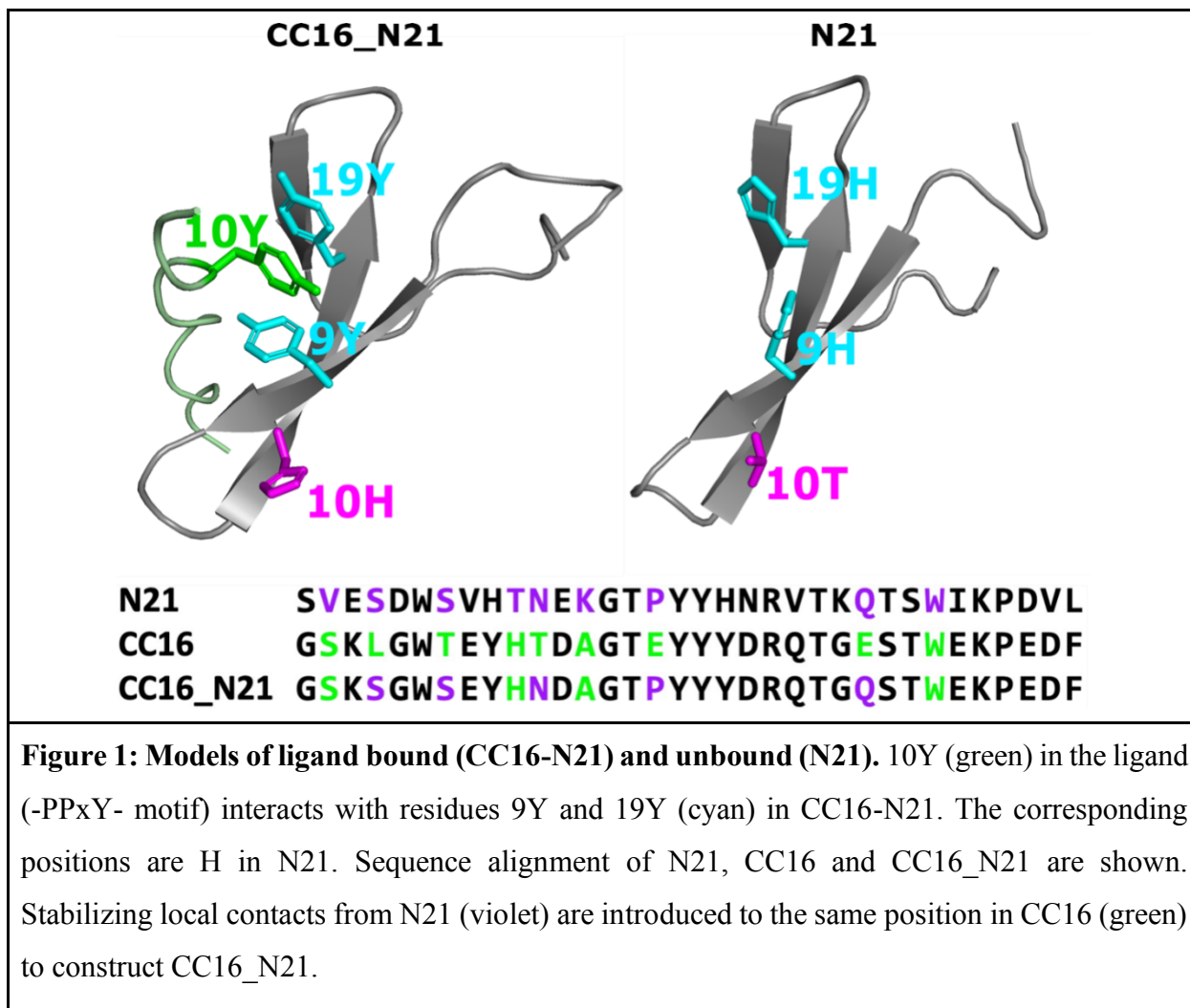
100

101 **Results and Discussion**

102 **Structure-based design of the variants considering the crucial contacts between the N21 and** 103 **the peptide.**

104 We investigated the molecular interaction governing peptide binding using modeled N21
105 and CC16-N21 peptide complexes, obtained through homology modelling¹⁸. The unbound
106 conformations were subjected to MD simulation and clustered using k-means to gather highly
107 sampled conformations²². The dominant conformation was used as input representative structure
108 for docking analyses with Adaptive BP-Dock to generate the bound complexes with the group 1
109 peptide. The docked pose with the lowest binding energy score was selected as the bound state
110 (Figure 1). The docked pose of CC16-N21 shows that tyrosine 9 and 19 are in contact with the
111 peptide ligand. These interactions are missing in N21 bound pose, which has two histidine at
112 positions 9 and 19. The difference in these interactions is reflected in the computed binding scores
113 of the complexes, -6.91 X-score energy units (XEU) for N21 and -7.62 XEU for CC16-N21
114 (Table 1), suggesting that these two residue positions are critical for binding to group 1 peptide.

115



117 **Dynamic-based design of the WW variant utilizing flexibility profiles.**

118 When we compare the flexibility profiles the N21 and CC16-N21, we observe that they
119 exhibit similar dynamics (Figure 2), except at positions 10 (histidine in CC16-N21 and threonine

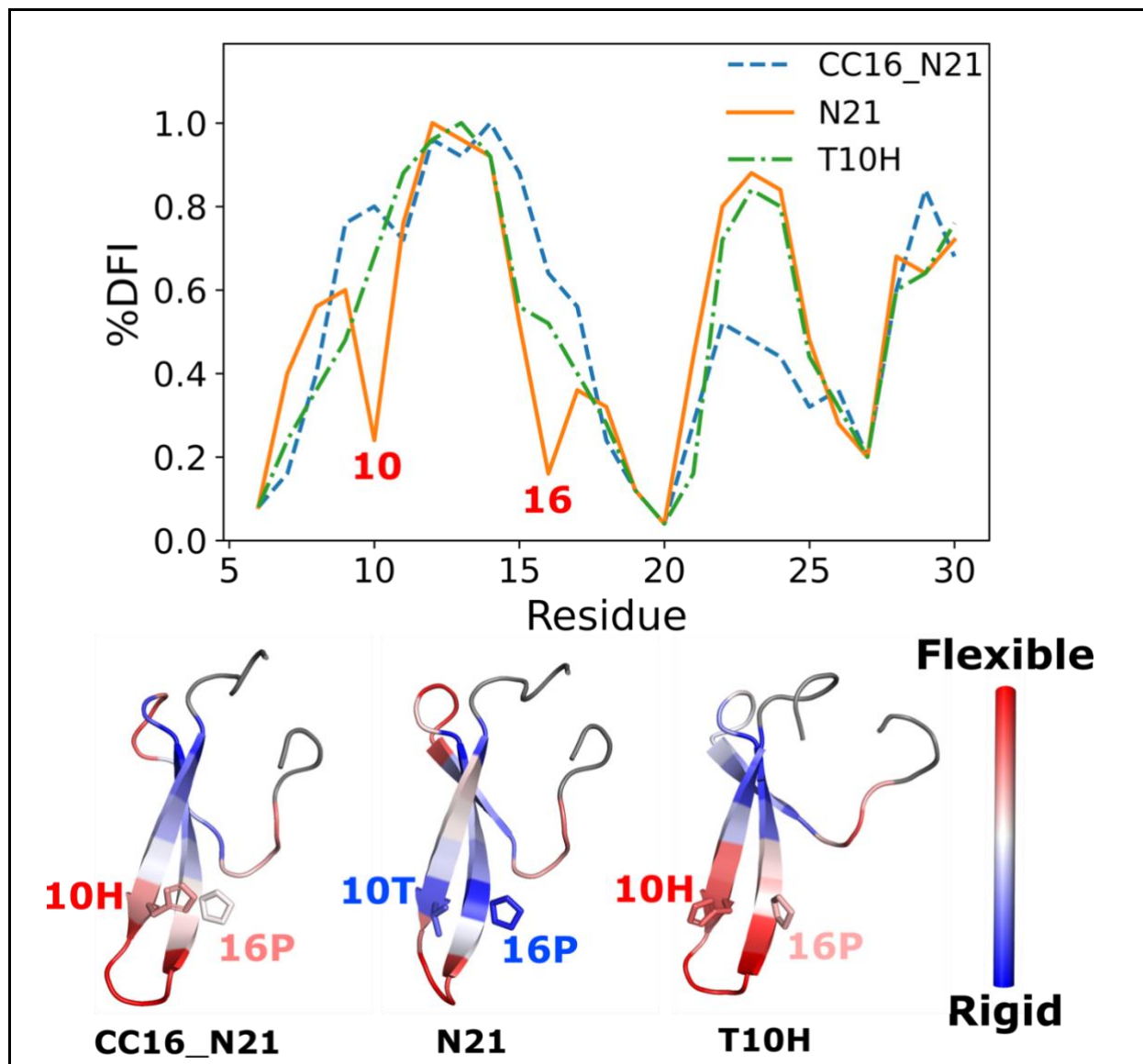


Figure 2: Dynamic-based design by comparing dynamic flexibility profile. DFI plots of N21, CC16-N21, and T10H (top) and color-coded ribbon diagrams showing DFI profile of each position (red, highest and blue, lowest DFI values). Positions 10 and 16, distal to the binding site, show hinge shifts that may contribute to binding. Residue position 16P is conserved. Mutating T10 to H in N21 restores the DFI profile towards that of CC16-N21, suggesting that T10H could modulate binding dynamics.

120 in N21) and 16 (proline in both), which appeared to be hinge shift positions. Based on other studies
121 suggesting the change in flexibility upon mutation (aka hinge shift mechanism) may impact
122 function, the change in dynamics of the two positions could be modulating factor of the difference
123 as seen in the peptide ligand binding

124 of CC16-N21 and N21¹⁸. To investigate this hinge shift mechanism in detail, we created a new
125 variant, T10H, by swapping the threonine with histidine in N21 and computed its changes in
126 dynamics and as well as binding energy score along with experimental characterizations. We found
127 that T10H mutation enhances the flexibility at positions 10 and 16 similar to that of CC16-N21.

128 **Biophysical characterization of the newly designed variants**

129 The mutants were prepared by recombinant expression and characterized experimentally.
130 We found that the mutations did not interfere with secondary structure formation, as shown by CD
131 spectroscopy. All mutants, H9Y, H19Y, H9YH19Y and T10H yielded CD spectra typical of the
132 WW fold and similar to WT N21, with a positive peak centered at 227 nm (Figure 3A). Thermal
133 denaturation experiments were carried out by monitoring the loss of CD signal at 227 nm in the 5
134 °C to 90 °C range (Figure 3B); the corresponding T_m values are summarized in Table 1. Mutants
135 H19Y (54.1 °C) and H9YH19Y (56.2 °C) are more stable to thermal denaturation than N21 (46.8

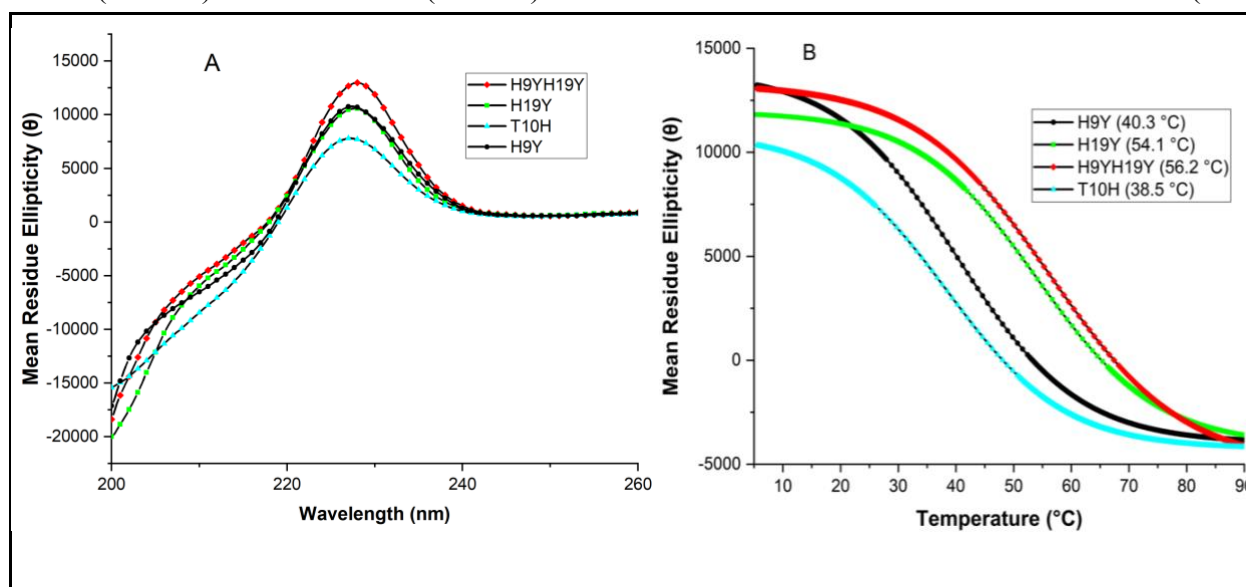


Figure 3: Structure foldability and thermostability of WW domain variants. A) CD scans of the WW domain variants at the far-UV wavelength (200nm-260nm). Folded variants show a signature peak at 227nm. B) Thermal denaturation (T_m) curves to measure the thermostability of the variants. Scans were taken at 227nm wavelength temperature ranging from 5°C to 90°C with a ramp rate of 0.3°C/min. Buffer condition: 20 mM NaPO₄ at pH 7.0.

136 °C), while mutations T10H (38.5 °C) and H9Y (40.3 °C) resulted in loss of stability compared to
137 N21, albeit within the range of naturally occurring WW sequences³. The proteins are monomeric
138 as assessed by size exclusion chromatography (SEC) at the concentrations used for binding assay

139 and concentration-dependent CD spectroscopy (Figure S2 and S3). Two-state folding is observed
140 as evidenced by the cooperative signal changes with well-defined linear pre- and post-transition
141 baselines²⁸ (Figure S6) and reversible transitions between folded and unfolded states with T_m
142 difference of 1.2 °C suggests the absence of intermediate species²⁹ (Figure S7).

143

144 **Restoration of the binding ability of N21 variants except for H19Y**

145 We assessed whether the designed variants bind group 1 proline-rich peptide by isothermal
146 titration calorimetry (ITC) titrations and compared the dissociation constants with CC16-N21, for
147 which a K_d of $71 \mu\text{M} \pm 4 \mu\text{M}$ had been measured¹⁸ (Table 1). We found that T10H and H9Y are
148 comparable to CC16-N21 (K_d of $84 \mu\text{M} \pm 1 \mu\text{M}$ and $86 \mu\text{M} \pm 6 \mu\text{M}$, respectively). (Figure 4A&4B).
149 H9YH19Y displayed improved binding ($K_d = 50 \mu\text{M} \pm 3 \mu\text{M}$) (Figure 4C) while H19Y did not
150 show any binding affinity for the ligand, even at 1mM concentration (Figure S4A & S4B). For
151 comparison, naturally occurring WW domains show a wide range of affinity towards group 1
152 peptide ranging from $1 \mu\text{M}$ to $500 \mu\text{M}$ ^{7,30}. We note that H9YH19Y retains the interactions between
153 tyrosine residues and proline residues of the peptide ligand observed in a variety of WW
154 domains^{31–33} and captured in the design of the original CC16 sequence based on MSA analysis¹⁸.

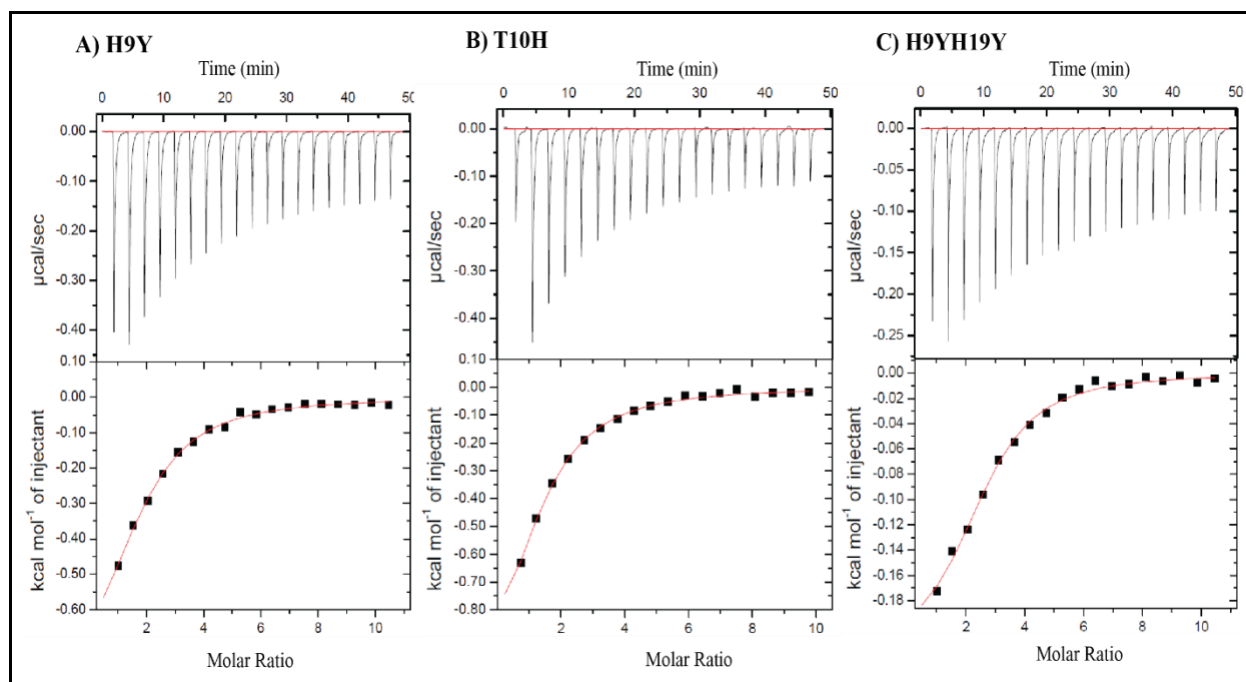


Figure 4: Isothermal Titration Calorimetry (ITC) for determining the binding affinity of the WW domain variants. The binding was assessed using group 1 peptide. Blank was done

using buffer only (Figure S4C) and each variant was assessed in duplicate. **A)** H9Y; **B)** T10H; and **C)** H9YH19Y. Buffer condition: 20 mM NaPO₄ at pH 7.0.

155 While the structural design H9Y and the double mutant H9YH19Y restored binding due to changes
 156 of interaction in the binding pocket led by the mutations at the binding site, the dynamic design
 157 T10H restored binding allosterically by retaining the same binding pocket.

158 **Table 1: Predicted binding scores, thermostability, and binding assay profile of the WW**
 159 **domain variants were summarized below.**

WW variants	T _m (°C)	K _d (μM)	ΔH (kcal/mol)	-TΔS (kcal/mol)	ΔG (kcal/mol)	Binding Energy Score (XEU)
N21*	46.8	--	--	--	--	-6.91
CC16_N21**	22.4	71 ± 4.7	-3.5 ± 0.2	-1.3 ± 0.0	-5.2± 0.1	-7.62
H9Y	40.3	86 ± 6.0	-0.9 ± 0.0	-4.3 ± 0.0	-5.2± 0.1	-7.62
H19Y	54.1	--	--	--	--	-6.88
H9YH19Y	56.2	50 ± 3.0	-0.2 ± 0.0	-5.3 ± 0.0	-5.5± 0.0	-8.03
T10H	38.5	84 ± 1.0	-1.2 ± 0.1	-4.0 ± 0.1	-5.2± 0.1	-7.63

160 *Naturally occurring variants used as background sequence for this study

161 **Variants used in previous studies¹⁸ and used for comparison in this study.

162
 163 Mirroring our previous observation with the parent sequences CC16-N21 and N21, the
 164 experimental binding affinities to group 1 peptide do not correlate with thermodynamic stability
 165 of the N21 mutant series. To understand the determinants of binding we applied Adaptive BP-dock
 166 and used X-score energy units (XEUs) as our binding criterion to differentiate binders from non-
 167 binders. N21 and H19Y have binding scores higher than -7.00 XEUs while H9Y, T10H,
 168 H9YH19Y, and CC16-N21 were lower than -7.62 XEUs (Figure 5A). A clear separation of binding
 169 scores lies between the binders and non-binders, which verifies the effectiveness of Adaptive BP-
 170 dock in investigating binding¹⁹. The predicted binding scores correlate well with the experimental
 171 binding equilibrium constants, K_d (Figure 5A & Table 1). Additionally, we examined the MD
 172 simulations of the unbound variants to understand the dynamics of residues that form the binding
 173 surface in WW domains. We utilized DFI metric to examine the total change in dynamics of these
 174 binding residues with respect to the non-binder N21 (Figure 5B). Variant H9YH19Y had the

175 largest change in the negative direction, indicating the highest level of rigidification compared to
 176 the others. In contrast, H19Y exhibited a change in the positive direction, suggesting that the
 177 hydrogen bonding residues are more flexible and therefore struggle maintaining interactions with
 178 the peptide, resulting in a loss of binding.

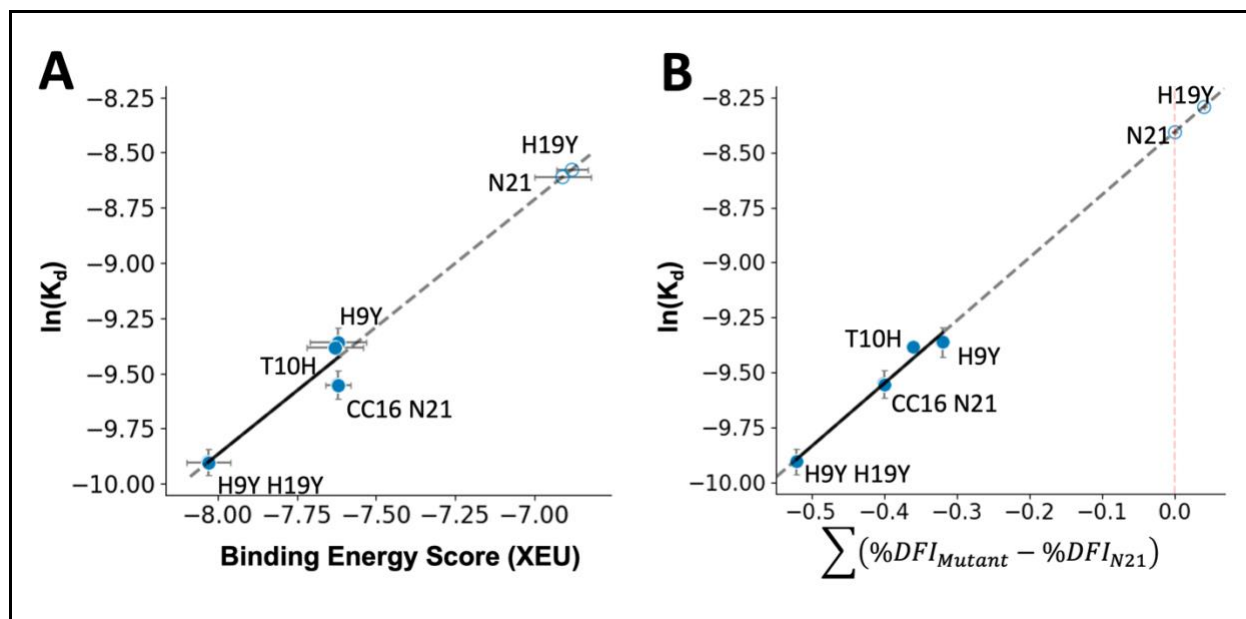


Figure 5: Experimental binding data compared with predicted binding score and change in %DFI of binding residues: A) Experimental binding $\ln(K_d)$ data collected with ITC shows that N21 and H19Y are non-binders while H9Y, T10H, H9YH19Y, and CC16-N21 are binders. The linear fit for both panels is created by using binders. The empty circles (non-binders) are the prediction from the fits. It shows a correlation ($R=0.94$) with predicted binding scores obtained from Adaptive BP-dock. The double mutant H9YH19Y has the lowest predicted binding energy score. N21 and H19Y are predicted to be non-binders. B) The change in dynamics ($\sum (\%DFI_{Mutant} - \%DFI_{N21})$) of binding residues which make hydrogen bonds with the peptide was investigated. The trend captures the experimental studies ($R=0.98$). The variant H9YH19Y has the largest change in the negative direction indicating the largest rigidification at the binding site compared to others. H19Y shows a change in the positive direction implying that the hydrogen bonding residues are more flexible which makes it harder to maintain the interactions with the peptide leading to loss of binding.

179
 180 Previous SCA analysis of WW domain revealed that eight positions show strong mutual
 181 co-evolution with the binding sites⁷. Some of these positions have no direct interactions with the
 182 ligands, suggesting that a distal dynamic allosteric mechanism might be governing the WW
 183 domain binding process. We explored whether there are possible allosteric substitutions in CC16-
 184 N21 that modulate binding affinity by applying DFI, a position-specific metric that measures the
 185 relative flexibility of a residue backbone compared with the rest of the protein. Flexible regions

186 identified by DFI metric tend to have a relatively large residue fluctuation response to a
187 perturbation on other regions, while rigid regions have lower responses. Rigid regions with a DFI
188 score lower than 0.2 are defined as hinges. These hinge sites have critical network of interactions
189 within the 3-D fold. They do not exhibit high residue response fluctuations to the perturbations
190 exerted on the protein chain, yet they can transfer the perturbations efficiently to the distal sites of
191 protein, like joints in a skeleton, and play a critical role in modulating the collective motion of a
192 protein. Hinges are critical to protein function: for example, mutations in these positions alter the
193 conformational dynamics profile and correlate to disease-associated mutations in ferritin²⁵. More
194 broadly, DFI profiles are associated with function and changes in DFI value, particularly in rigid
195 sites, leads to changes in function^{34,35}. Comparative dynamics analysis of ancestral proteins with
196 their corresponding extant homologs revealed that change in DFI profile, particularly
197 compensation of the loss of certain hinge locations by the formation of the new hinge sites called
198 a hinge-shift mechanism, is utilized by nature to manipulate protein function²⁴. The DFI analysis
199 of Human Pin1 also showed that substrate binding to the WW domain induces a hinge shift
200 mechanism and enhances the catalytic efficiency³⁶.

201 Hydrogen bonds are important interactions in biological systems, as they contribute to the
202 stability and function of proteins and other biomolecules. Thus, we analyzed the number of
203 hydrogen bond patterns of the docked poses and computed the number of hydrogen bonds formed
204 between the peptide ligand and the binding residues for each mutant (Figure 6). We found that
205 CC16-N21 and H9YH19Y formed five hydrogen bonds, H9Y and T10H had four hydrogen bonds,
206 and only one hydrogen bond was identified for the nonbinders N21 and H19Y. This analysis also
207 aligns with our dynamics analysis and suggests that the enhanced flexibility of these binding
208 residues in N21 and H19Y lead to loss in the formation of hydrogen bonds, thus leading to poor
209 binding affinity.

210

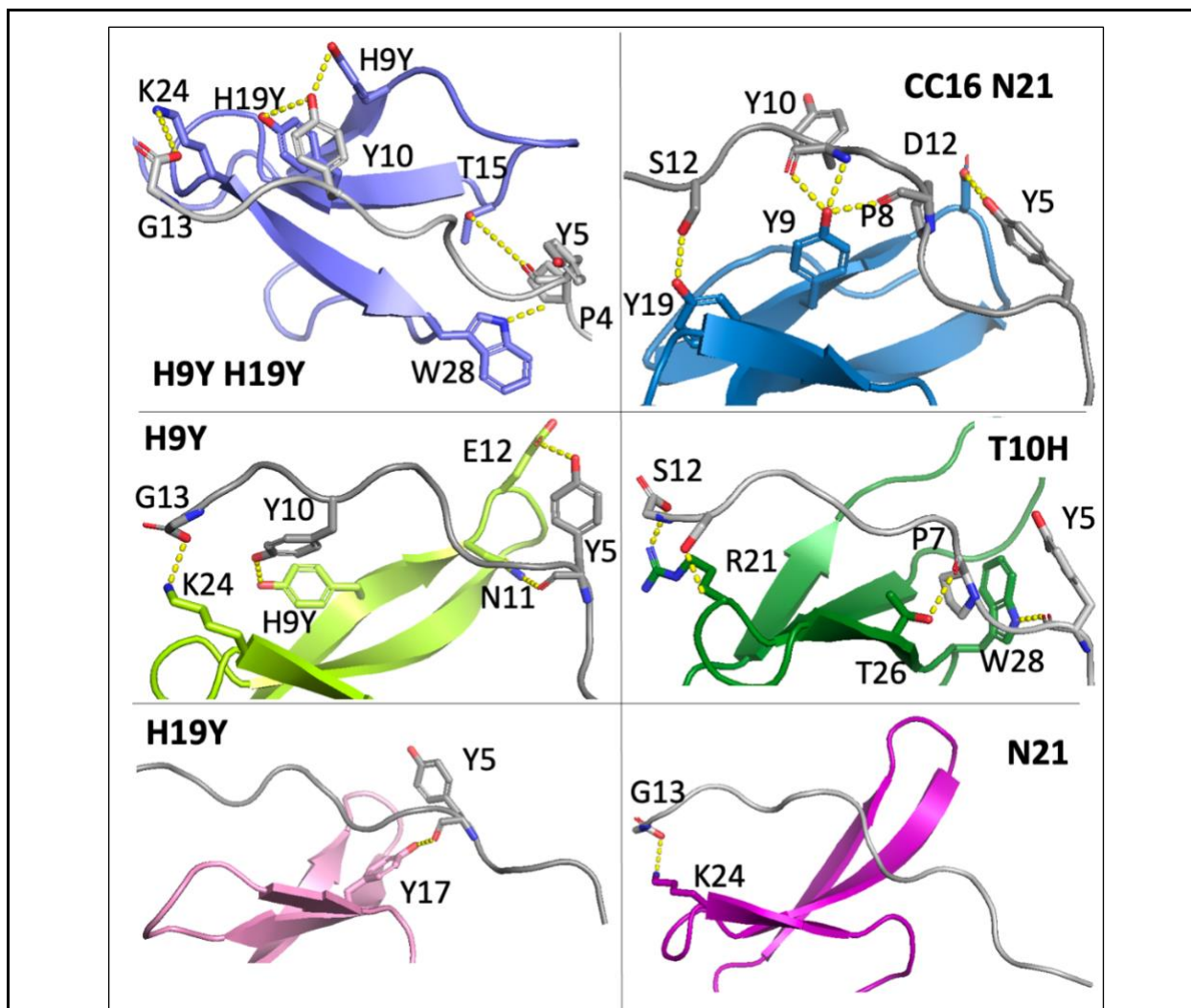


Figure 6: Docking poses of the WW domain variants showing H-bonding. The docked poses of CC16-N21, H9YH19Y, N21, H9Y, H19Y, and T10H are shown in cartoon representations. Residues making hydrogen bonding interactions with the peptide ligand (gray) are shown in sticks and annotated in the figure. Hydrogen bonds (yellow dashes) between the peptide ligand and the residues of the protein are highlighted. Five hydrogen bonds are observed for CC16-N21 and H9YH19Y. H9Y and T10H only make four hydrogen bonds with the peptide ligand. Only one hydrogen bond is identified for the nonbinders N21 and H19Y.

211
 212 Since our results strongly support that the dynamics of WW domain play a critical role in
 213 its biophysical properties, we further investigated the equilibration and the relaxation of dynamics
 214 of variants. Thus, we studied %DFI in a sequential manner by creating a time series which carries

215 information on the evolution of the dynamics. We prepared the time series %DFI by averaging 3
 216 adjacent time windows respectively ($0.5\mu\text{s}$ - $1\mu\text{s}$, $1\mu\text{s}$ - $1.5\mu\text{s}$, and $1.5\mu\text{s}$ - $2\mu\text{s}$). As our earlier
 217 works^{9,10,23,27} highlight that the DFI profiles capture the related function^{4,11,22,24,37-39}, we cluster
 218 these time series of the DFI values of each variant using PCA (See Methods) to compare their
 219 dynamics profiles. The first two principal components are responsible for most of the variance in
 220 the mutant DFI profiles. Hence, we utilized these two first principal components to analyze the
 221 clustering of the mutants based on their similarity in flexibility profiles. The projection of the data
 222 on the first and second principal components shows that the second principal component (PC_2)
 223 clearly separates binders and non-binders (Fig. 7A). All variants exhibiting binding to group 1
 224 peptide have positive PC_2 scores, indicating that they have similar flexibility profiles associated
 225 with binding dynamics. In contrast, H19Y is clustered with the native N21 with negative PC_2
 226 scores, suggesting that their unbound dynamics results in poor binding (Figure 7A). The first

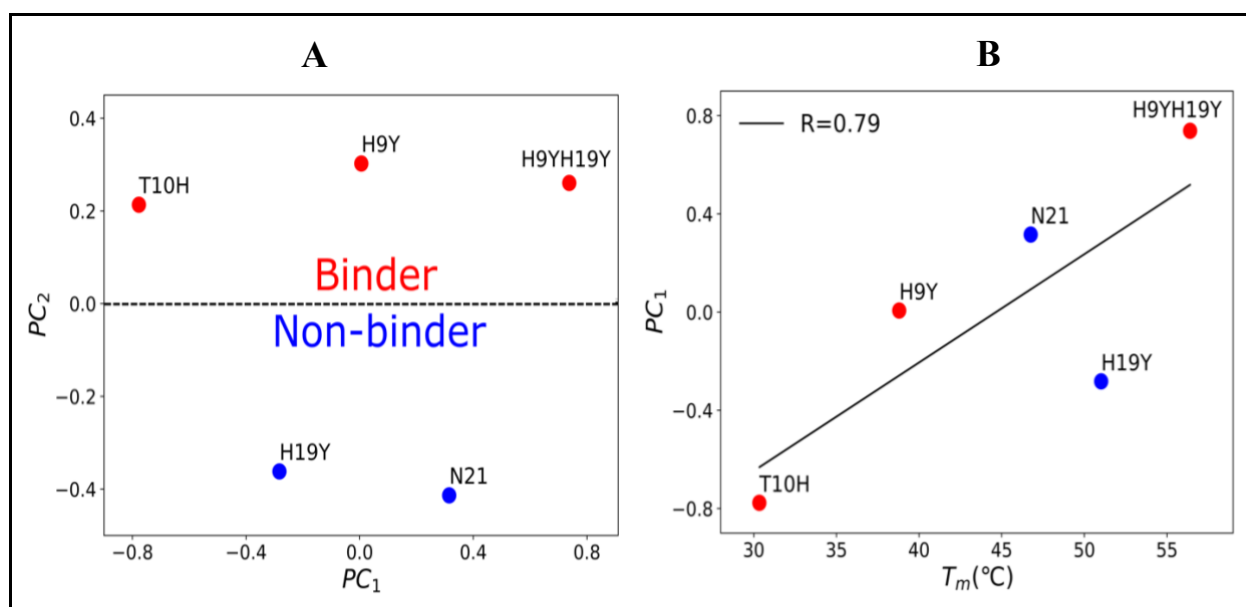


Figure 7: A) Correlation between PC_2 and binding affinity: The projections of times series DFI data on the first and second principal components show separation between binders (in red) and non-binders (in blue) on the second principal components score, where binders have $PC_2 > 0$ and non-binders have $PC_2 < 0$. **B) Correlation between PC_1 and melting temperature (T_m):** The plot of PC_1 vs T_m shows a clearly positive correlation ($R=0.79$, $P=0.11$) between them, indicating that the PC_1 reflects the stability of N21 and its mutants.

227 principal component (PC₁) captures folding stability: its value is correlated with melting
228 temperature (T_m) (Figure 7B). This analysis differentiates the role of dynamics in modulating
229 protein stability and binding poses and can help explain why H19Y doesn't bind the ligand.

230 **Conclusion**

231 We conducted a comparative analysis of the WW domains N21 and CC16-N21 to explore
232 why N21 exhibits poor binding, while its close homolog, artificially designed CC16-N21, showed
233 high affinity to group 1 peptides. The peptide-bound structure obtained by adaptive BP-dock
234 highlighted differences in the binding domains between N21 and CC16-N21. Binding in CC16-
235 N21 is mediated by two tyrosine residues (9Y and 19Y) that contact the peptide, whereas in the
236 N21 sequence, the equivalent positions are occupied by histidine. We explored whether unbound
237 dynamics (i.e., the unbound conformational ensemble) played a major role in binding by
238 computing DFI profiles, which provide position-specific metrics related to conformational entropy
239 per site. The comparison of the DFI profiles suggested a hinge-shift point at a distal position 10,
240 which is a histidine in CC16-N21 but a threonine in N21. Based on these observations, we
241 generated four mutants of N21 by substituting these residues: H9Y, H19Y, T10H, and the double
242 mutant H9YH19Y. The bound forms were modeled using Adaptive BP-Dock and ranked
243 according to their docking energy scores. The variants were experimentally characterized: all
244 formed secondary structures comparable to N21, although mutations modulated the stability to
245 thermal denaturation. Furthermore, the binding affinities to group 1 peptide correlated with the
246 predicted docking energy scores. When we coupled this analysis with the computed DFI values of
247 the positions that formed hydrogen bonds with the peptide, we observed that enhanced flexibility
248 at these binding residue positions correlated with impaired binding in N21 and H19Y. Principal
249 component analysis of time-series DFI sheds light on the role of unbound dynamics in governing
250 binding and stability. These results suggest that dynamics govern WW domain binding, and that
251 sites that do not directly interact but distally modulate the dynamics of binding may also be crucial
252 and fundamental for binding. We hope that our structure and dynamics-based protein design
253 approach can be used to predict protein binding in general and to study protein-ligand interactions.

254

255 **Methods and Materials**

256 **Molecular Dynamics Simulation**

257 Molecular dynamics simulations of the wild-type and mutants were performed using
258 AMBER 20⁴⁰. The mutants were modeled by PyMOL Mutagenesis Wizard⁴¹. Topology files were
259 prepared based on ff99SB forcefield and the solvation box was modeled by explicit water model
260 TIP3P⁴² with a 14 Å minimum distance from the boundary to protein. The systems were
261 neutralized by adding sodium and chloride ions and then minimized with the steepest descent
262 algorithm followed by the conjugate gradient method for 5000 steps. The systems were then heated
263 up to 300 K. Each system was then simulated for 2 μs with 2 fs time-step at constant temperature
264 (300 K) and pressure (1 bar) with Langevin thermostat and barostat.

265 **Adaptive BP-dock**

266 Adaptive BP-dock^{9,19} is an iterative docking approach that utilizes perturbation response
267 scanning (PRS)⁴³ combined with the RosettaLigand program (version 3.5)⁴⁴ to model the
268 interactions between the WW domain and the peptide ligand. The induced fit that emerged from
269 the binding event is challenging to model with docking tools with static protein backbone and
270 peptide movement. In Adaptive BP-Dock, we include both the backbone flexibility of the receptor
271 and the ligand. Before each docking step, a new conformation of the protein receptor is calculated
272 based on the residue response fluctuation profile upon force perturbations on the binding pocket
273 residues using PRS. This approach mimics the peptide ligand's forces acting on the receptor and
274 generates a new conformation that samples binding-induced conformations. This conformation is
275 then docked with the peptide ligand using RosettaLigand. Adaptive BP-dock which includes
276 binding-induced backbone conformational changes improves the modeling of binding interactions
277 and can predict binding scores that capture the binding trends seen in experiments. The predicted
278 binding scores are evaluated by X-score empirical scoring function. X-score energy units (XEU) have
279 shown previously to provide good correlation with experimental results^{19,45,46}. Thus, we
280 applied Adaptive BP-dock to each of the most representative clusters sampled during unbound
281 MD simulations. We conducted three separate docking simulations to ensure the binding
282 interactions between the WW domain and peptide ligand are captured accurately.

283 **Dynamic Flexibility Index**

284 Dynamic Flexibility Index^{4,9,24,25,27,37,38,47} uses the PRS technique that combines Elastic
285 Network Model (ENM) and Linear Response Theory (LRT)²¹. In PRS, Brownian-like unit forces
286 F are applied sequentially to each residue as perturbations^{25,43}. According to LRT, the linear

287 response vector perturbation ΔR due to F is calculated as following where H^{-1} is the inverse of
 288 Hessian matrix.

$$289 \quad [\Delta R]_{3N \times 1} = [H]_{3N \times 3N}^{-1} [F]_{3N \times 1} \quad (1)$$

290

291 In this work, instead of using Hessian matrix calculated via ENM, we used covariance matrix G
 292 for C-alpha atoms calculated from MD trajectories which is proportional to the inverse of the
 293 Hessian matrix (H^{-1}). This is because MD provides more precise residue-residue interaction, such
 294 as long-range interactions and solvation effects via atomistic force fields.

$$295 \quad [\Delta R]_{3N \times 1} = [G]_{3N \times 3N} [F]_{3N \times 1} \quad (2)$$

296

297 To compute DFI, we perturbed each residue sequentially by applying random unit forces on each
 298 residue. We then generated Perturbation Responses Matrix \mathbf{A} as following.

$$299 \quad A_{N \times N} = [|\Delta R^1|_1 \cdots |\Delta R^N|_1 \quad \vdots \quad |\Delta R^1|_N \cdots |\Delta R^N|_N] \quad (3)$$

300

301 where $|\Delta R^j|_i = \sqrt{\langle (\Delta R)^2 \rangle}$ denotes the average response at position i due to perturbations on j .

302 This procedure is repeated several times in different directions for each position, to ensure that
 303 forces are isotropically sampled. Then the averaged Perturbation Response Matrix \mathbf{A} is used to
 304 calculate the DFI per residue.

$$305 \quad DFI_i = \frac{\sum_{j=1}^N |\Delta R^j|_i}{\sum_{i=1}^N \sum_{j=1}^N |\Delta R^j|_i} \quad (4)$$

306

307 This index is often more useful as a percentile, since the DFI range varies for different proteins.
 308 Therefore, DFI percentile is calculated as

$$309 \quad \%DFI_i = \frac{n_{\leq i}}{N} \quad (5)$$

310 where N is the total number of residues and $n_{\leq i}$ is the number of residues with DFI value $\leq DFI_i$.

311 To understand and capture the converged dynamics of the protein system, we calculated time series
 312 $\%DFI_i$ based on MD covariance matrices from the three sequential time windows: (i) 0.5 μ s-1 μ s,
 313 (ii) 1 μ s-1.5 μ s and (iii) 1.5 μ s-2 μ s. To improve the accuracy, the loose ends of the proteins were
 314 excluded.

315 **Principal Component Analysis**

316 Principal component analysis (PCA) was applied to time series DFI. This dimensionality-
 317 reduction method is used to reduce the variables in a high dimensional dataset while retaining most

318 of the information from the dataset, therefore making the data more interpretable⁴⁸. For N21 and
319 its mutants, the time series DFI profiles were merged into $n \times p$ matrix X where $n = 5$ (total
320 number of DFI profiles) and $p = 75$ (dimension of time series DFI)²². Singular value
321 decomposition of X was conducted as follows:

$$322 \quad [X]_{n \times p} = [U]_{n \times n} [\Sigma]_{n \times p} [V]_{p \times p}^T \quad (6)$$

323
324 Here U and V are unitary matrices with orthonormal columns which are called left singular vectors
325 and right singular vectors, respectively. Σ is a rectangular diagonal matrix of positive number σ_i
326 called the singular values of X . σ_i were arranged, by convention, in a decreasing order of their
327 magnitude and represents the variances in the corresponding left and right singular vectors.

328 The column vectors of V is called the principal components. They are new variables that are
329 constructed from the initial variables where first principal component is a direction which
330 maximizes the variance of the projected data, therefore preserves most of the data's variation.
331 Score matrix T is defined as follows:

$$332 \quad [T]_{n \times p} = [U]_{n \times n} [\Sigma]_{n \times p} \quad (7)$$

333
334 Each row vector of T is the projection of the corresponding data vector from matrix X on every
335 principal component. In this study, we utilized the projections of our original data vectors on the
336 first and second principal components and discovered their relations with the protein functions.

337 **Plasmid sequencing and protein expression**

338 The sequences encoding for the designed WW domain proteins, containing point
339 mutation(s) on N21 native sequence, were ordered from Genscript. All mutants were fused to
340 Maltose Binding Protein (MBP) and cloned in pMAL-c5x vector for expression. Each gene
341 contained an N-terminal poly-histidine tag and the TEV cleavage site ENLYFQG to facilitate
342 purification. The plasmids were transformed via heat shock into competent *E. coli* BL-21 cells
343 (NEB) and the mix were plated on LB agar plates containing ampicillin overnight at 37 °C. Single
344 colonies were used to inoculate 5 mL LB liquid cultures containing ampicillin and were grown
345 overnight at 37 °C shaking at 200 RPM. 10 mL of each culture was transferred to a 2 L flask
346 containing 1 L LB media with ampicillin for growth and expression. The rest of the cells were
347 centrifuged down, and the plasmid DNA was extracted using Promega Wizard[®] Plus SV Miniprep
348 kits. Sequences were verified using GeneWiz Sanger Sequencing. The 1 L cultures were grown to

349 OD₆₀₀ of 0.6-0.8 and protein expression was induced by addition of 1mM IPTG. Proteins were
350 expressed for 6 hours at 37 °C shaking at 200 RPM. Total protein yield for these conditions was
351 roughly 20 mg/L.

352 **Protein isolation and purification**

353 Cells were harvested by centrifugation at 5,000 RPM for 20 minutes and resuspended in
354 30 mL 20 mM NaPO₄ at pH 7.4, 0.5 M NaCl, and 20 mM imidazole buffer. Cells were lysed by
355 sonication for 20 minutes using ON/OFF cycle by 30 seconds, and then spun down at 5,000 RPM,
356 4 °C for 1 hour. The supernatant was purified on a 5 mL Amersham Bioscience HisTrap column
357 by FPLC (AKTApure). Fractions containing the protein were dialyzed in 20 mM NaPO₄ at pH 7.4,
358 0.5 M NaCl, and 10 mM imidazole at 4 °C. The His-tag was cleaved by digesting the proteins with
359 TEV at a ratio of 1:20 TEV to fusion protein, followed by purification by HisTrap column; WW
360 proteins were collected in flowthrough. The proteins were further purified by RP-HPLC on a 250
361 x 10 mm Phenomenex C18 Semi-prep column by gradient elution starting with 0.01% TFA in
362 water (solvent A) to 95% acetonitrile with 0.01% TFA (solvent B). Purified proteins were verified
363 by MALDI (Figure S5) and stored at -20 °C after being lyophilized.

364 **group 1 peptide synthesis and purification**

365 Proline rich peptide, group 1, was synthesized on a CEM Liberty automated peptide
366 synthesizer using Wang resin and Fmoc protected amino acids. Deprotection conditions: 20%
367 Piperidine, 0.1M HOBT in DMF. Activation and coupling solutions: 0.5 M HBTU and 2M DIEA
368 in NMP. After completion of the synthesis, cleavage from resin was accomplished by shaking for
369 2 hours using a cleavage cocktail containing 95% TFA, 2.5% Triisopropylsilane, and 2.5%
370 distilled water. After 2 hours, the mixture was filtered, excess TFA removed, and lyophilized. The
371 crude peptide was purified by RP-HPLC on a 250 x 10 mm Phenomenex C18 Semi-prep column
372 by gradient elution starting with 0.01% TFA in water (solvent A) to 95% acetonitrile with 0.01%
373 TFA (solvent B). and verified by MALDI (Bruker).

374 **Circular Dichroism**

375 Protein stability and folding was assessed by Circular Dichroism (CD) using a JASCO J-
376 815 CD Spectrophotometer (JASCO, Easton, MD). Full scans were measured from 280 nm-200
377 nm at 5 °C with a 1cm (or 1mm) quartz cuvette, at protein concentration of 40 μM in 20 mM
378 NaPO₄ buffer at pH 7.4. Spectra were collected in triplicate, averaged, and converted to mean
379 residue ellipticity using the following formula.

380
$$\text{Mean Residue Ellipticity}(\theta) = \frac{Mdeg * M}{10 * L * C * n} \quad (8)$$

381 Here, Mdeg= millidegree; M= molecular weight of the protein (g/mol); n= number of amino acids;
382 L= path length of the cuvette (cm); C= concentration of the protein (g/L)
383 Denaturation temperature (T_m) for all the WW domain peptides were calculated by monitoring
384 ellipticity at 227 nm while increasing temperature from 5 °C to 90 °C at a ramp rate of 0.3°C/min.
385 The reported T_m is the inflection point of the sigmoidal curve and is calculated using the Boltzmann
386 sigmoid equation.

387
$$Y = \frac{(LL + (UL - LL))}{\frac{(1 - \exp(Tm - X))}{Slope}} \quad (9)$$

388 where UL and LL are the values of minimum and maximum intensities, respectively^{49,50}. Data
389 generated from variable temperature was processed using OriginPro 2018.

390 **Isothermal Titration Calorimetry (ITC)**

391 WW domain and group 1 peptides were sent to Sanford-Burnham Medical Research
392 Institute (La Jolla, CA) for ITC using an ITC200 calorimeter from Microcal (North Hampton,
393 MA). In short, aliquots of group 1 peptide from a 5 mM stock were titrated into 100 μM WW
394 domain peptides, in 20 mM NaPO₄ buffer, pH 7.0. Data were analyzed using standard fitting
395 procedures with a one-binding site model and analyzed using the Origin software package
396 provided by Microcal. Titrations were carried out in duplicates, using phosphate buffer as blank.
397

398 **References**

- 399
400 (1) Russ, W. P.; Figliuzzi, M.; Stocker, C.; Barrat-Charlaix, P.; Socolich, M.; Kast, P.;
401 Hilvert, D.; Monasson, R.; Cocco, S.; Weigt, M.; Ranganathan, R. An Evolution-Based Model
402 for Designing Chorismate Mutase Enzymes. *Science* **2020**, *369* (6502), 440–445.
403 <https://doi.org/10.1126/science.aba3304>.
404 (2) Jiang, X.-L.; Dimas, R. P.; Chan, C. T. Y.; Morcos, F. Coevolutionary Methods Enable
405 Robust Design of Modular Repressors by Reestablishing Intra-Protein Interactions. *Nat.*
406 *Commun.* **2021**, *12* (1), 5592. <https://doi.org/10.1038/s41467-021-25851-6>.
407 (3) Socolich, M.; Lockless, S. W.; Russ, W. P.; Lee, H.; Gardner, K. H.; Ranganathan, R.
408 Evolutionary Information for Specifying a Protein Fold. *Nature* **2005**, *437* (7058), 512–518.
409 <https://doi.org/10.1038/nature03991>.
410 (4) Butler, B. M.; Kazan, I. C.; Kumar, A.; Ozkan, S. B. Coevolving Residues Inform Protein
411 Dynamics Profiles and Disease Susceptibility of NSNVs. *PLOS Comput. Biol.* **2018**, *14* (11),
412 e1006626. <https://doi.org/10.1371/journal.pcbi.1006626>.

413 (5) Bai, F.; Morcos, F.; Cheng, R. R.; Jiang, H.; Onuchic, J. N. Elucidating the Druggable
414 Interface of Protein–protein Interactions Using Fragment Docking and Coevolutionary Analysis.
415 *Proc. Natl. Acad. Sci.* **2016**, *113* (50). <https://doi.org/10.1073/pnas.1615932113>.

416 (6) Hopf, T. A.; Ingraham, J. B.; Poelwijk, F. J.; Schärfe, C. P. I.; Springer, M.; Sander, C.;
417 Marks, D. S. Mutation Effects Predicted from Sequence Co-Variation. *Nat. Biotechnol.* **2017**, *35*
418 (2), 128–135. <https://doi.org/10.1038/nbt.3769>.

419 (7) Russ, W. P.; Lowery, D. M.; Mishra, P.; Yaffe, M. B.; Ranganathan, R. Natural-like
420 Function in Artificial WW Domains. *Nature* **2005**, *437* (7058), 579–583.
421 <https://doi.org/10.1038/nature03990>.

422 (8) Voelz, V. A.; Shell, M. S.; Dill, K. A. Predicting Peptide Structures in Native Proteins
423 from Physical Simulations of Fragments. *PLoS Comput. Biol.* **2009**, *5* (2), e1000281.
424 <https://doi.org/10.1371/journal.pcbi.1000281>.

425 (9) Kazan, I. C.; Sharma, P.; Rahman, M. I.; Bobkov, A.; Fromme, R.; Ghirlanda, G.; Ozkan,
426 S. B. Design of Novel Cyanovirin-N Variants by Modulation of Binding Dynamics through
427 Distal Mutations. *eLife* **2022**, *11*, e67474. <https://doi.org/10.7554/eLife.67474>.

428 (10) Modi, T.; Campitelli, P.; Kazan, I. C.; Ozkan, S. B. Protein Folding Stability and Binding
429 Interactions through the Lens of Evolution: A Dynamical Perspective. *Curr. Opin. Struct. Biol.*
430 **2021**, *66*, 207–215. <https://doi.org/10.1016/j.sbi.2020.11.007>.

431 (11) Campitelli, P.; Swint-Kruse, L.; Ozkan, S. B. Substitutions at Nonconserved Rheostat
432 Positions Modulate Function by Rewiring Long-Range, Dynamic Interactions. *Mol. Biol. Evol.*
433 **2021**, *38* (1), 201–214. <https://doi.org/10.1093/molbev/msaa202>.

434 (12) Sudol, M.; Hunter, T. NeW Wrinkles for an Old Domain. *Cell* **2000**, *103* (7), 1001–1004.
435 [https://doi.org/10.1016/S0092-8674\(00\)00203-8](https://doi.org/10.1016/S0092-8674(00)00203-8).

436 (13) Sudol, M. Structure and Function of the WW Domain. *Prog. Biophys. Mol. Biol.* **1996**,
437 *65* (1–2), 113–132. [https://doi.org/10.1016/S0079-6107\(96\)00008-9](https://doi.org/10.1016/S0079-6107(96)00008-9).

438 (14) Ilsley, J. L.; Sudol, M.; Winder, S. J. The WW Domain: Linking Cell Signalling to the
439 Membrane Cytoskeleton. *Cell. Signal.* **2002**, *14* (3), 183–189. [https://doi.org/10.1016/S0898-6568\(01\)00236-4](https://doi.org/10.1016/S0898-6568(01)00236-4).

440 (15) Chen, H. I.; Sudol, M. The WW Domain of Yes-Associated Protein Binds a Proline-Rich
441 Ligand That Differs from the Consensus Established for Src Homology 3-Binding Modules.
442 *Proc. Natl. Acad. Sci.* **1995**, *92* (17), 7819–7823. <https://doi.org/10.1073/pnas.92.17.7819>.

443 (16) Rotin, D. WW (WWP) Domains: From Structure to Function; 1998; pp 115–133.
444 https://doi.org/10.1007/978-3-642-80481-6_5.

445 (17) Macias, M. J.; Hyvönen, M.; Baraldi, E.; Schultz, J.; Sudol, M.; Saraste, M.; Oschkinat,
446 H. Structure of the WW Domain of a Kinase-Associated Protein Complexed with a Proline-Rich
447 Peptide. *Nature* **1996**, *382* (6592), 646–649. <https://doi.org/10.1038/382646a0>.

448 (18) Zou, T.; W. Woodrum, B.; Halloran, N.; Campitelli, P.; A. Bobkov, A.; Ghirlanda, G.;
449 Banu Ozkan, S. Local Interactions That Contribute Minimal Frustration Determine Foldability.
450 *J. Phys. Chem. B* **2021**, *125* (10), 2617–2626. <https://doi.org/10.1021/acs.jpcc.1c00364>.

451 (19) Bolia, A.; Ozkan, S. B. Adaptive BP-Dock: An Induced Fit Docking Approach for Full
452 Receptor Flexibility. *J. Chem. Inf. Model.* **2016**, *56* (4), 734–746.
453 <https://doi.org/10.1021/acs.jcim.5b00587>.

454 (20) Bolia, A.; Woodrum, B. W.; Cereda, A.; Ruben, M. A.; Wang, X.; Ozkan, S. B.;
455 Ghirlanda, G. A Flexible Docking Scheme Efficiently Captures the Energetics of Glycan-
456 Cyanovirin Binding. *Biophys. J.* **2014**, *106* (5), 1142–1151.
457 <https://doi.org/10.1016/j.bpj.2014.01.040>.

458

459 (21) Nevin Gerek, Z.; Kumar, S.; Banu Ozkan, S. Structural Dynamics Flexibility Informs
460 Function and Evolution at a Proteome Scale. *Evol. Appl.* **2013**, *6* (3), 423–433.
461 <https://doi.org/10.1111/eva.12052>.

462 (22) Kolbaba-kartchner, B.; Can Kazan, I.; Mills, J. H.; Banu Ozkan, S. The Role of Rigid
463 Residues in Modulating TEM-1 β -Lactamase Function and Thermostability. *Int. J. Mol. Sci.*
464 **2021**, *22* (6), 1–19. <https://doi.org/10.3390/ijms22062895>.

465 (23) Butler, B. M.; Gerek, Z. N.; Kumar, S.; Ozkan, S. B. Conformational Dynamics of
466 Nonsynonymous Variants at Protein Interfaces Reveals Disease Association. *Proteins Struct.*
467 *Funct. Bioinforma.* **2015**, *83* (3), 428–435. <https://doi.org/10.1002/prot.24748>.

468 (24) Modi, T.; Risso, V. A.; Martinez-Rodriguez, S.; Gavira, J. A.; Mebrat, M. D.; Van Horn,
469 W. D.; Sanchez-Ruiz, J. M.; Banu Ozkan, S. Hinge-Shift Mechanism as a Protein Design
470 Principle for the Evolution of β -Lactamases from Substrate Promiscuity to Specificity. *Nat.*
471 *Commun.* **2021**, *12* (1), 1852. <https://doi.org/10.1038/s41467-021-22089-0>.

472 (25) Kumar, A.; Glembo, T. J.; Ozkan, S. B. The Role of Conformational Dynamics and
473 Allostery in the Disease Development of Human Ferritin. *Biophys. J.* **2015**, *109* (6), 1273–1281.
474 <https://doi.org/10.1016/j.bpj.2015.06.060>.

475 (26) Modi, T.; Huihui, J.; Ghosh, K.; Ozkan, S. B. Ancient Thioredoxins Evolved to Modern-
476 Day Stability–Function Requirement by Altering Native State Ensemble. *Philos. Trans. R. Soc.*
477 *B Biol. Sci.* **2018**, *373* (1749), 20170184–20170184. <https://doi.org/10.1098/rstb.2017.0184>.

478 (27) Larrimore, K. E.; Kazan, I. C.; Kannan, L.; Kendle, R. P.; Jamal, T.; Barcus, M.; Bolia,
479 A.; Brimijoin, S.; Zhan, C.-G.; Ozkan, S. B.; Mor, T. S. Plant-Expressed Cocaine Hydrolase
480 Variants of Butyrylcholinesterase Exhibit Altered Allosteric Effects of Cholinesterase Activity
481 and Increased Inhibitor Sensitivity. *Sci. Rep.* **2017**, *7* (1), 10419. <https://doi.org/10.1038/s41598-017-10571-z>.

483 (28) Jäger, M.; Nguyen, H.; Crane, J. C.; Kelly, J. W.; Gruebele, M. The Folding Mechanism
484 of a β -Sheet: The WW Domain. *J. Mol. Biol.* **2001**, *311* (2), 373–393.
485 <https://doi.org/10.1006/jmbi.2001.4873>.

486 (29) Koepf, E. K.; Petrassi, H. M.; Sudol, M.; Kelly, J. W. WW: An Isolated Three-Stranded
487 Antiparallel β -Sheet Domain That Unfolds and Refolds Reversibly; Evidence for a Structured
488 Hydrophobic Cluster in Urea and GdnHCl and a Disordered Thermal Unfolded State. *Protein*
489 *Sci.* **2008**, *8* (4), 841–853. <https://doi.org/10.1110/ps.8.4.841>.

490 (30) Kato, Y.; Nagata, K.; Takahashi, M.; Lian, L.; Herrero, J. J.; Sudol, M.; Tanokura, M.
491 Common Mechanism of Ligand Recognition by Group II/III WW Domains. *J. Biol. Chem.* **2004**,
492 *279* (30), 31833–31841. <https://doi.org/10.1074/jbc.M404719200>.

493 (31) Kraemer-Pecore, C. M.; Lecomte, J. T. J.; Desjarlais, J. R. A de Novo Redesign of the
494 WW Domain. *Protein Sci.* **2009**, *12* (10), 2194–2205. <https://doi.org/10.1110/ps.03190903>.

495 (32) Macias, M. J.; Wiesner, S.; Sudol, M. WW and SH3 Domains, Two Different Scaffolds
496 to Recognize Proline-Rich Ligands. *FEBS Lett.* **2002**, *513* (1), 30–37.
497 [https://doi.org/10.1016/S0014-5793\(01\)03290-2](https://doi.org/10.1016/S0014-5793(01)03290-2).

498 (33) Hu, H.; Columbus, J.; Zhang, Y.; Wu, D.; Lian, L.; Yang, S.; Goodwin, J.; Luczak, C.;
499 Carter, M.; Chen, L.; James, M.; Davis, R.; Sudol, M.; Rodwell, J.; Herrero, J. J. A Map of WW
500 Domain Family Interactions. *PROTEOMICS* **2004**, *4* (3), 643–655.
501 <https://doi.org/10.1002/pmic.200300632>.

502 (34) Xu, Y.; Colletier, J.-P.; Weik, M.; Jiang, H.; Moulton, J.; Silman, I.; Sussman, J. L.
503 Flexibility of Aromatic Residues in the Active-Site Gorge of Acetylcholinesterase: X-Ray versus

504 Molecular Dynamics. *Biophys. J.* **2008**, *95* (5), 2500–2511.
505 <https://doi.org/10.1529/biophysj.108.129601>.

506 (35) Teilum, K.; Olsen, J. G.; Kragelund, B. B. Functional Aspects of Protein Flexibility. *Cell.*
507 *Mol. Life Sci.* **2009**, *66* (14), 2231–2247. <https://doi.org/10.1007/s00018-009-0014-6>.

508 (36) Campitelli, P.; Guo, J.; Zhou, H.-X.; Ozkan, S. B. Hinge-Shift Mechanism Modulates
509 Allosteric Regulations in Human Pin1. *J. Phys. Chem. B* **2018**, *122* (21), 5623–5629.
510 <https://doi.org/10.1021/acs.jpcc.7b11971>.

511 (37) Ose, N. J.; Butler, B. M.; Kumar, A.; Kazan, I. C.; Sanderford, M.; Kumar, S.; Ozkan, S.
512 B. Dynamic Coupling of Residues within Proteins as a Mechanistic Foundation of Many
513 Enigmatic Pathogenic Missense Variants. *PLoS Comput. Biol.* **2022**, *18* (4), e1010006.
514 <https://doi.org/10.1371/journal.pcbi.1010006>.

515 (38) Stevens, A. O.; Kazan, I. C.; Ozkan, B.; He, Y. Investigating the Allosteric Response of
516 the PICK1 PDZ Domain to Different Ligands with All-Atom Simulations. *Protein Sci.* **2022**, *31*
517 (12), e4474. <https://doi.org/10.1002/pro.4474>.

518 (39) Zou, T.; Risso, V. A.; Gavira, J. A.; Sanchez-Ruiz, J. M.; Ozkan, S. B. Evolution of
519 Conformational Dynamics Determines the Conversion of a Promiscuous Generalist into a
520 Specialist Enzyme. *Mol. Biol. Evol.* **2015**, *32* (1), 132–143.
521 <https://doi.org/10.1093/molbev/msu281>.

522 (40) Salomon-Ferrer, R.; Götz, A. W.; Poole, D.; Le Grand, S.; Walker, R. C. Routine
523 Microsecond Molecular Dynamics Simulations with AMBER on GPUs. 2. Explicit Solvent
524 Particle Mesh Ewald. *J. Chem. Theory Comput.* **2013**, *9* (9), 3878–3888.
525 <https://doi.org/10.1021/ct400314y>.

526 (41) DeLano, W. L. The PyMOL Molecular Graphics System; [Http://www.pymol.org](http://www.pymol.org).
527 *PyMOL Mol. Graph. Syst.* **2002**.

528 (42) Mark, P.; Nilsson, L. Structure and Dynamics of the TIP3P, SPC, and SPC/E Water
529 Models at 298 K. *J. Phys. Chem. A* **2001**, *105* (43), 9954–9960.
530 <https://doi.org/10.1021/jp003020w>.

531 (43) Atilgan, C.; Gerek, Z. N.; Ozkan, S. B.; Atilgan, A. R. Manipulation of Conformational
532 Change in Proteins by Single-Residue Perturbations. *Biophys. J.* **2010**, *99* (3), 933–943.
533 <https://doi.org/10.1016/j.bpj.2010.05.020>.

534 (44) Meiler, J.; Baker, D. ROSETTALIGAND: Protein-Small Molecule Docking with Full
535 Side-Chain Flexibility. *Proteins Struct. Funct. Bioinforma.* **2006**, *65* (3), 538–548.
536 <https://doi.org/10.1002/prot.21086>.

537 (45) Bolia, A.; Gerek, Z. N.; Ozkan, S. B. BP-Dock: A Flexible Docking Scheme for
538 Exploring Protein–Ligand Interactions Based on Unbound Structures. *J. Chem. Inf. Model.* **2014**,
539 *54* (3), 913–925. <https://doi.org/10.1021/ci4004927>.

540 (46) Wang, R.; Lai, L.; Wang, S. Further Development and Validation of Empirical Scoring
541 Functions for Structure-Based Binding Affinity Prediction. *J. Comput. Aided Mol. Des.* **2002**, *16*
542 (1), 11–26. <https://doi.org/10.1023/A:1016357811882>.

543 (47) Gerek, Z. N.; Ozkan, S. B. Change in Allosteric Network Affects Binding Affinities of
544 PDZ Domains: Analysis through Perturbation Response Scanning. *PLoS Comput. Biol.* **2011**, *7*
545 (10), e1002154. <https://doi.org/10.1371/journal.pcbi.1002154>.

546 (48) Jolliffe, I. T.; Cadima, J. Principal Component Analysis: A Review and Recent
547 Developments. *Philos. Trans. R. Soc. Math. Phys. Eng. Sci.* **2016**, *374* (2065), 20150202.
548 <https://doi.org/10.1098/rsta.2015.0202>.

- 549 (49) Niesen, F. H.; Berglund, H.; Vedadi, M. The Use of Differential Scanning Fluorimetry to
550 Detect Ligand Interactions That Promote Protein Stability. *Nat. Protoc.* **2007**, *2* (9), 2212–2221.
551 <https://doi.org/10.1038/nprot.2007.321>.
- 552 (50) Orwig, S. D.; Lieberman, R. L. Biophysical Characterization of the Olfactomedin
553 Domain of Myocilin, an Extracellular Matrix Protein Implicated in Inherited Forms of
554 Glaucoma. *PLoS ONE* **2011**, *6* (1), e16347. <https://doi.org/10.1371/journal.pone.0016347>.
555